PROCEEDINGS, Thirty-Fifth Workshop on Geothermal Reservoir Engineering
Stanford University, Stanford, California, February 1-3, 2010
SGP-TR-188

HYDRAULIC FRACTURING PROPAGATION IN HETEROGENEOUS ROCK USING THE VMIB METHOD

Kyoung Suk Min, Zhennan Zhang, Ahmad Ghassemi

Harold Vance Department of Petroleum Engineering, Texas A&M University,
3116 TAMU College Station, TX 77840, USA
e-mail: kyoung.min@pe.tamu.edu
ahmad.ghassemi@pe.tamu.edu

ABSTRACT

Hydraulic fracturing in rock often takes a complex form involving multiple fracture propagation resulting from material and stresses heterogeneity. Formation of multiple cracks and crack branching phenomena cause high fracture tortuosity and increased treatment pressure. In this paper, crack propagation by hydraulic pressurization is investigated using the Virtual Multidimensional Internal Bond (VMIB). Especially, multiple cracks and crack branching behavior near wellbore are simulated in both homogeneous and inhomogeneous rock. In addition, multiple fracturing is studied with reference to the role of material and stress inhomogeneity, and fracture interactions.

INTRODUCTION

Better understanding and control of crack branching during hydraulic fracturing is essential for both geothermal and petroleum industries in order to enhance reservoir connectivity. Characterization of multiple crack growth in heterogeneous rock is more complex than conventional crack propagation in homogeneous rock. Previous fracture models have serious difficulties in simulating crack growth, especially, when the path of fracture is not known as *a priori*. Recently, Klein and Gao(Gao and Klein 1997) proposed a virtual internal bond (VIB) model with cohesive interactions between material particles as an alternative approach to modeling fracture. Because the fracture process involves atomic interactions at the microscale, the VIB model(Klein and Gao 1998) incorporates the cohesive description of particle interactions from an atomic view of material in order to introduce fracture criterion directly into the continuum constitutive behavior. Zhang et al (Zhang and Ge 2005) introduced the virtual multidimensional internal bonds (VMIB) model by adding rotational dimensions to the VIB model to account for shear effect of the particles. In this paper, a poroelastic VMIB is developed and validated. In addition, the poroelastic VMIB model is extended to include rock heterogeneity. The model is used simulated behavior of multiple fracture propagation during hydraulic fracturing in heterogeneous rock.

VMIB MODEL

Zhang et al(Zhang and Ge 2005) proposed the Virtual Multidimensional Internal Bonds (VMIB) models to exhibit fracture mechanism using the cohesive laws incorporated directly into the constitutive models. The VMIB model reproduces the behavior of a homogeneous, hyperelastic solid which has a microstructure consisting of internal cohesive bonds between networks of material particles. The potential of a unit cell of material particles can be expressed as(Zhang and Ge 2006)

$$\Phi = \int_0^{2\pi}\int_0^{\pi} U_L D(\theta,\phi)\sin(\theta)\,d\theta d\phi + \int_0^{2\pi}\int_0^{\pi} (U_{R1}+U_{R2}+U_{R3})\,D(\theta,\phi)\sin(\theta)\,d\theta d\phi \tag{1}$$

where $U_L, U_{Ri}\,(i=1,2,3)$ are respectively, the potential contributions of normal stiffness and shear stiffness of bond. $D(\theta,\varphi)$ is the spatial distribution density of bond.

$$U_L = \frac{1}{2}\lambda\bar{k}\left(\xi_i\varepsilon_{ij}\xi_j\right)^2, U_{R1} = \frac{1}{2}\lambda\bar{r}\left(\xi_i\varepsilon_{ij}\eta_j^{'}\right)^2, \quad U_{R2} = \frac{1}{2}\lambda\bar{r}\left(\xi_i\varepsilon_{ij}\eta_j^{''}\right)^2, U_{R3} = \frac{1}{2}\lambda\bar{r}\left(\xi_i\varepsilon_{ij}\eta_j^{'''}\right)^2 \tag{2}$$

where $\eta^{'} = \xi\times(\vec{x}_1\times\xi), \eta^{''} = \xi\times(\vec{x}_2\times\xi), \eta^{'''} = \xi\times(\vec{x}_3\times\xi)$
The mean value of $\bar{k}, \bar{r}$ can be determined by

$$\bar{k} = \frac{3E}{4\pi(1-2\nu)}, \quad \bar{r} = \frac{3(1-4\nu)E}{4\pi(1+\nu)(1-2\nu)} \tag{3}$$

The elastic tensor of the unit cell is derived using the hyperelastic theory. For the two-dimensional case, the elastic tensor expression is:

$$C_{ijmn} = \int_0^{\pi} \left(\lambda \bar{k} \xi_i \xi_j \xi_m \xi_n + \lambda \bar{r} \xi_i \eta_j' \xi_m \eta_n' + \lambda \bar{r} \xi_i \eta_j'' \xi_m \eta_n'' \right) D(\theta) \, d\theta \quad (4)$$

where $\xi = (\cos\theta, \sin\theta)$ $\eta' = (-\sin\theta, \cos\theta)$; $\eta'' = (\sin\theta, -\cos\theta)$
The bond evolution governs the macro mechanical response of material. The following bond evolution form is proposed(Zhang and Chen 2008):

$$\begin{Bmatrix} \bar{k} \\ \bar{r} \end{Bmatrix} = \begin{Bmatrix} \bar{k}_0 \\ \bar{r}_0 \end{Bmatrix} \exp\left(-c \cdot \delta^n\right) \quad (5)$$

c and *n* are model parameters which govern the features of stress-strain response of materials. They can be calibrated by fitting the results from a uniaxial compression test on the material. δ is defined as"

$$\delta = \frac{\ell}{\varepsilon_t} + \frac{\beta}{0.5(1+\nu)\varepsilon_t} \quad (6)$$

where $\ell = \left| \xi_i \varepsilon_{ij} \xi_j \right|, \beta = \left| \xi_i \varepsilon_{ij} \eta_j \right|$
Since flaws and dislocations initiate the crack in material, bond density in this softening region decreases when the deformation caused by the flaws and dislocations exceed the linear elastic limit. In the linear elastic phase, both the L-bond and the R-bond density are kept constant. So, L-bond density is expressed as

$$D_L(\theta, \phi) = \begin{cases} \dfrac{1}{4\pi} & l' \le \varepsilon_c \\ \dfrac{1}{4\pi} \exp\left[-\lambda \left(l' - \varepsilon_c \right)^2 / \varepsilon_c \right] & l' > \varepsilon_c \end{cases} \quad (7)$$

where ε_c is the critical value of strain. This critical value is determined by experimental data. λ is a coefficient used to adjust the reduction ratio of bond density.

POROELASTIC VMIB MODEL

A poroelastic VMIB has been developed by Zhang and Ghassemi(Zhang and Ghassemi 2010). The approach uses Biot's pore pressure diffusion equation and couples it to the solid stresses as follow:

$$\begin{aligned} \frac{\partial \sigma_x'}{\partial x} + \frac{\partial \tau_{xy}}{\partial y} - \alpha \frac{\partial p}{\partial x} = 0 \\ \frac{\partial \tau_{xy}}{\partial x} + \frac{\partial \sigma_y'}{\partial y} - \alpha \frac{\partial p}{\partial y} = 0 \end{aligned} \quad (8)$$

where p is the pore pressure; σ_x' and σ_y' are the effective stress, $\sigma_x' = \sigma_x - \alpha p$, $\sigma_y' = \sigma_y - \alpha p$.
The hydraulic diffusivity equation is:

$$-\alpha \frac{d\varepsilon_{ii}}{dt} + \frac{k}{\mu} \nabla^2 p = \frac{1}{M} \frac{\partial p}{\partial t} \quad (9)$$

where $\varepsilon_{ii} = \dfrac{\partial u}{\partial x} + \dfrac{\partial v}{\partial y}$; α is Biot's coefficient; μ is the viscosity of fluid; k is the permeability; M is the Biot's modulus.
For simplified FEM formulation, the coupled mechanical equilibrium equation could be described in matrix form as:

$$\begin{bmatrix} K_t & C \\ C^T & -\Delta t \cdot S - V \end{bmatrix} \begin{bmatrix} U_t \\ P_t \end{bmatrix} = \begin{bmatrix} 0 & 0 \\ C^T & -V \end{bmatrix} \begin{bmatrix} U_0 \\ P_0 \end{bmatrix} + \begin{bmatrix} F_t \\ 0 \end{bmatrix} \quad (10)$$

where K is the so-called stiffness matrix of element,

$$K = \iint_s \left(L_{3\times2} N_{2\times6} \right)^T D_{3\times3} L_{3\times2} N_{2\times6} \, dxdy;$$

$$C = \alpha \iint_s N_{6\times2}^T \tilde{L}_{2\times1} \tilde{N}_{1\times3} \, dxdy;$$

$$S = \frac{k}{\mu} \iint_s \left(\tilde{L}_{2\times1} \tilde{N}_{1\times3} \right)^T \tilde{L}_{2\times1} \tilde{N}_{1\times3} \, dxdy;$$

$$V = \frac{1}{M} \iint_s \tilde{N}_{3\times1}^T \tilde{N}_{1\times3} \, dxdy$$

where $D_{3\times3}$ is the constitutive stress-strain matrix, L is a partial differential operator, N is the shape function matrix, Δt is the time interval.

VERIFICATION OF POROELASTIC VMIB

The coupled consolidation problem (Biot 1941) is used as a test case for the numerical algorithms and the poroelastic implementation. General assumptions are isotropy of the material, reversibility of stress-strain relations under final equilibrium conditions, linearity of stress-strain relations, small strains, and the validity of Darcy's law. The simplified analytical solution was suggested as following (Biot 1941):

$$\begin{aligned} w_s &= w_0 - w_i \\ &= \frac{8}{\pi^2} (a - a_i) h p_0 \sum_0^{\infty} \frac{1}{(2n+1)^2} \left\{ 1 - \exp\left[1 \left(\frac{(2n+1)\pi}{2h} \right)^2 ct \right] \right\} \end{aligned} \quad (11)$$

$$\sum_0^{\infty} \frac{1}{(2n+1)^2} = \frac{\pi^2}{8}, w_i = a_i h p_0 \quad (12)$$

$$\frac{1}{c} = \alpha^2 \frac{a}{k} + \frac{1}{Qk} \tag{13}$$

$$a = \frac{1-2\nu}{2G(1-\nu)}, a_i = \frac{a}{1+\alpha^2 aQ} \tag{14}$$

Consolidation of an elastic solid in plane strain using 3-node triangular is compared with analytical solution given by Biot(Biot 1941). Bottom of simulation domain was restricted in the X-Y directions and both sides are only restricted in X-direction. Pore-pressure boundary of the top surface is set to zero where compression is applied. Initial pressure applied on the top surface is $p = 1MPa$. The material parameters for the rock are given in Table 1.

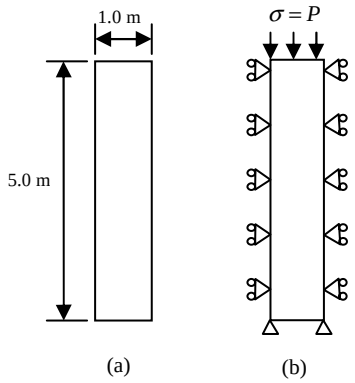

Figure 1: One Dimensional Biot consolidation
(a) Dimension of specimen
(b) Boundary Conditions

Table 1: Material parameters

E	ν	k	M	Viscosity
1.0 GPa	0.2	1e-7 md	1e3 MPa	1

Verification for Homogeneous rock

The comparison between the numerical and analytical results for the displacement of the top surface is shown in Fig. 2. It is seen that the numerical results have good agreement with the analytical solution. Also, the results show that the appropriate time step size Δt depends on the material properties. A higher permeability needs a smaller time step $(\Delta t = 0.001s)$, while for lower permeability rocks a larger step $(\Delta t = 1000s)$ is more suitable for accurate solution. In Fig. 2c, the soft rock which has small Young's modulus requires large step size $(\Delta t = 1000s)$ than the hard rock. Thus, an appropriate time step is essential for efficiency in computation cost and time.

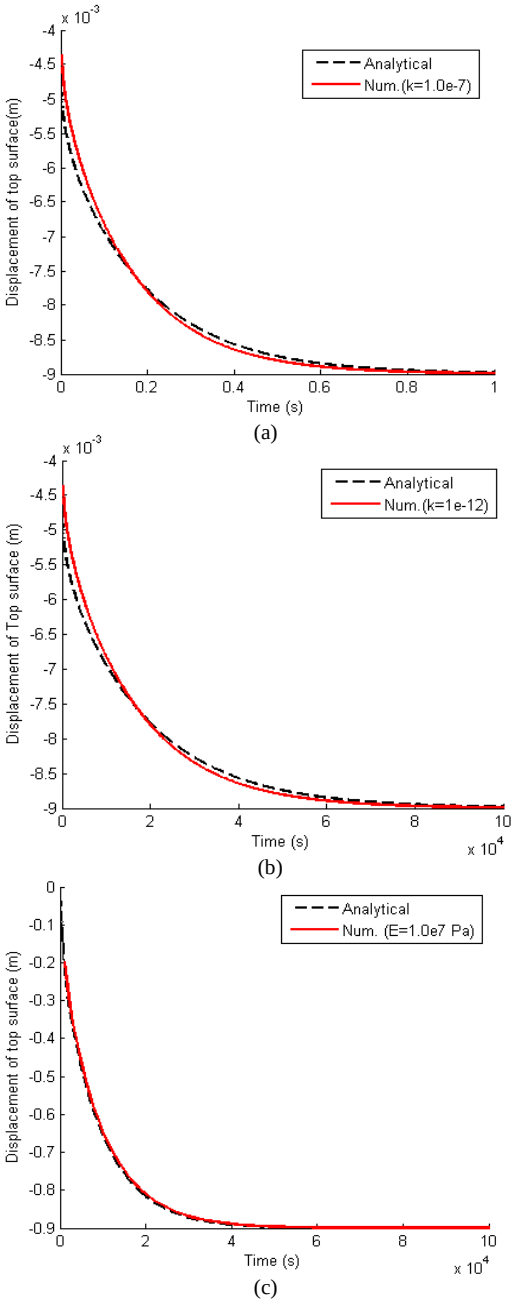

Figure 2: Comparison of displacement of the top surface. (a) High Permeability (k=1.0e-7md, Δt =0.001s); (b) Low Permeability (k=1.0e-12md, Δt =1000s); (c) Soft rock (E=1.0e-3 GPa, Δt =1000s).

Consideration of Rock Heterogeneity

Rock is a heterogeneous material and this heterogeneity can lead to the formation of multiple cracks and crack branching during fracture propagation. In order to take into account rock heterogeneity, a statistical technique is used to represent a distribution of material properties. In general, the Weibull distribution function is

applicable for modeling failure of rock (Fang and Harrison 2002). Failure process of rock is complex, so a statistical model of heterogeneity should be able to sufficiently account for a variety of possibilities. However, it is difficult to explain all cases since different materials require different statistical models (Wong et al. 2006). The Weibull distribution is widely used in several areas including survival analysis, weather forecasting, and failure analysis(Weibull 1951) because of the flexibility of its variables. The Weibull distribution is defined by the following probability density function (Weibull 1939):

$$f(m) = \frac{a}{m_0}\left(\frac{m}{m_0}\right)^{a-1} \exp\left[-\left(\frac{m}{m_0}\right)^{a}\right] \qquad (15)$$

where m_0 is the mean value of the random variable, m and the parameter a determines the shape of the distribution function. A random variable m for heterogeneity is generated using Weibull distribution with parameters m_0 and a. A value of $m_0 > 1$ indicates hard heterogeneity which represents smaller displacement. On the other hand, a value of $m_0 < 1$ indicates soft heterogeneity which represents larger displacement in Fig. 4.

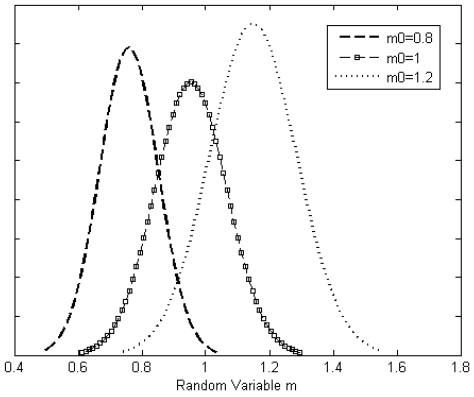

Figure 3: Distribution curves of random Variable.

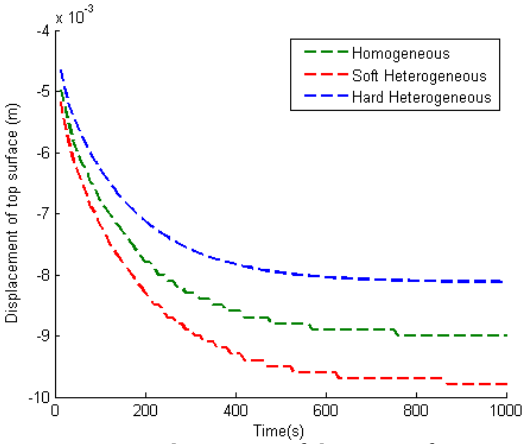

Figure 4: Displacements of the top surface

Fig. 3 shows the distribution curves of different random variables with the same parameter $a = 6$. In Fig. 4, a soft heterogeneous rock that has small mean value of random variable $(m_0 = 0.8)$ experiences a large displacement at the top surface and hard heterogeneous rock with large mean value of random variable $(m_0 = 1.2)$ has a smaller surface displacement.

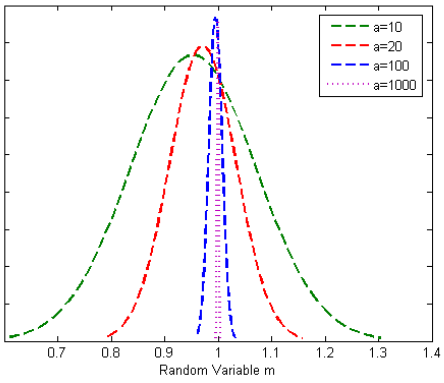

(a)

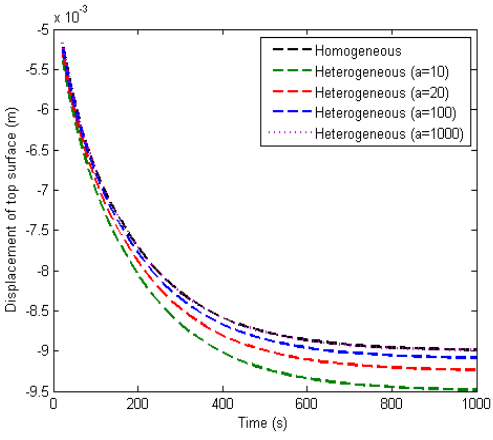

(b)

Figure 5: Comparison of Simulation results. (a) Distribution curves of random variables; (b) Displacement at the top

There are two ways to apply the Weibull distribution for considering heterogeneity in the poroelastic VMIB model namely, the stiffness controlled method and strain/strength controlled method. In this paper, the stiffness controlled method is used because it is easier to use for representing heterogeneity than the stain/strength controlled method. Fig. 5 shows that heterogeneity decreases as a becomes large, so that a material with large a approaches homogeneity. In Fig. 5b, the behavior of the stiffness controlled heterogeneity is shown in Biot's consolidation. It is seen that a high heterogeneity level reduces the rock stiffness causing larger displacements. Fig. 5b also indicates that the Weibull distribution function is implemented correctly in the FEM.

SIMULATION OF FAILURE IN HETEROGENEOUS ROCK

Failure under drained uniaxial compression

In this section, modeling of mechanical breakdown in intact heterogeneous rock is simulated using the poroelastic VMIB model developed above. Young's modulus $(E = 10GPa)$ and Poisson ratio $(\nu = 0.2)$ representing a sandstone are used. For heterogeneity of the specimen, Weibull distribution function given by $m_0 = 1$ and $a = 6$ is used. A compressive stress of 5 MPa is initially applied on top of the specimen and is then gradually increased by 0.1KPa increments. A time step of $\Delta t = 10s$ is used.

Table 2: Material parameters

E	ν	k	M	Viscosity
10 GPa	0.2	1e-10 md	1e3 MPa	1

In Fig. 6, results of failure simulation show that crack initiates at t=3420s and propagates thorough an inclined plane. Dispersion of strain concentration in the rock is a characteristic behavior of heterogeneous material. Note that the failure simulation using the poroelastic VMIB has a form similar to those in other works (Yuan and Harrison 2006) shown in Fig. 7. Similar inclination of the failure planes is found in both Fig. 6 and 7.

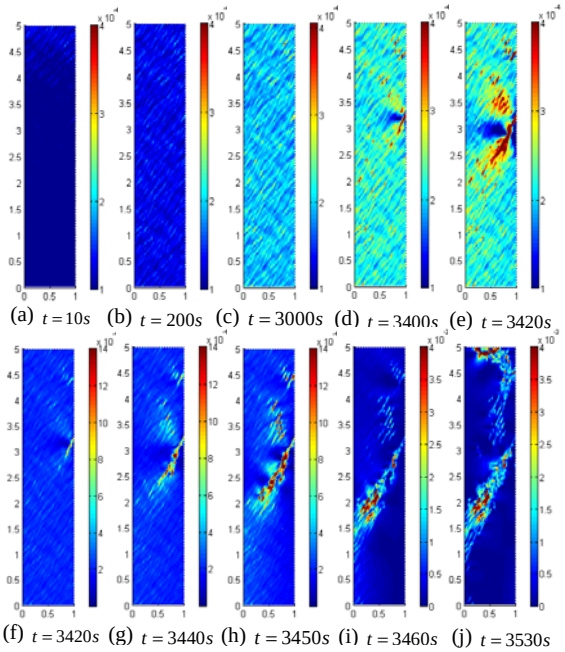

Figure 6: Simulation of strain concentration with crack propagation

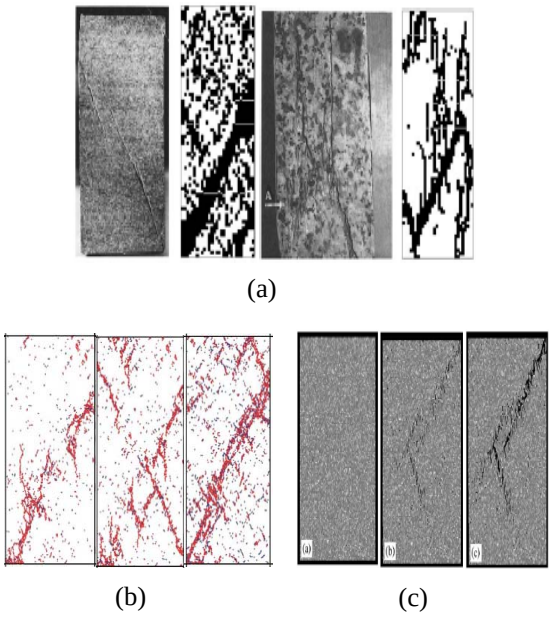

Figure 7: Failure simulation using other methods: (a) CDM based statistical models by the local degradation approach from Fang Z et al 200; (b) Particle based statistical model by microscopic damage from Potyondy et al 2004; (c) CDM based statistical models by the coupled flow-stress-damage model from Tang et al 2002.

Failure under undrained uniaxial compression

Drained boundary conditions were applied to the sides and bottom surfaces in the previous example. Fig. 8 and 9 show the results for the case where undrained boundary condition is applied on all sides. According to the results, undrained boundary condition leads to high a value of axial effective stress required for crack initiation and propagation.

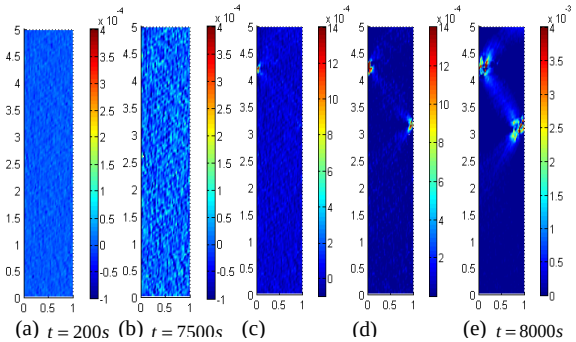

Figure 8: Distribution of strain concentration with crack propagation

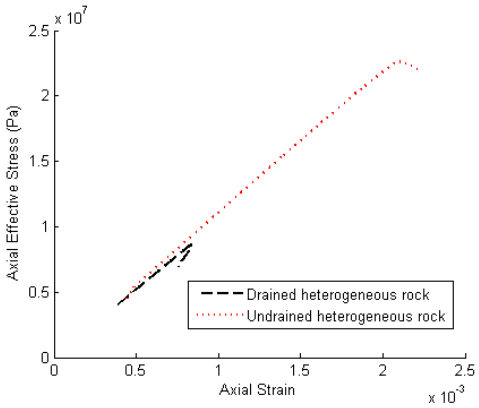

(a)

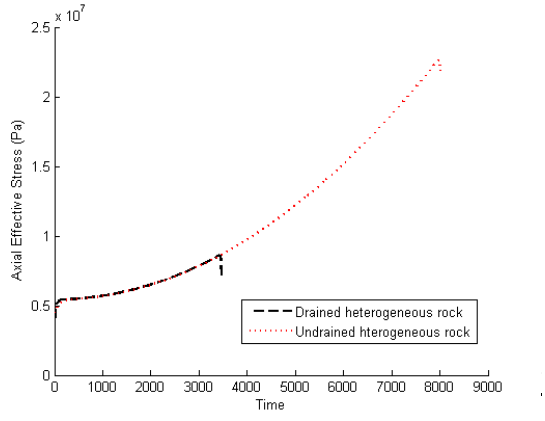

(b)

Figure 9: Undrained heterogeneous rock failure (a) Axial Effective stress curve with axial strain (b) Axial Effective stress curve with time

Several cases of hydraulic fracturing simulation are investigated in both homogeneous and heterogeneous rock formation. For a general study of hydraulic fracturing simulation, simplified numerical model and boundary condition is used as described in Fig. 10. A reservoir dimension of $(x = 30m, y = 30m)$ and initial perforated crack length of $(l = 1m)$ are assumed to study the behavior of crack direction induced by hydraulic fracturing. The mechanical properties of the rock are shown in Table 2. A uniform mesh was used to distribute heterogeneity equally in each of the 16,200 elements used to simulate fracture propagation. A fined mesh and small time step are needed to capture multiple fracturing phenomenon (Thiagarajan et al. 2003). Hydraulic pressure was applied to the crack at the center of the numerical domain and is gradually increased an amount Δp. Weibull distribution parameters are set to $m_0 = 1.2$ and $a = 10$ to represent heterogeneity.

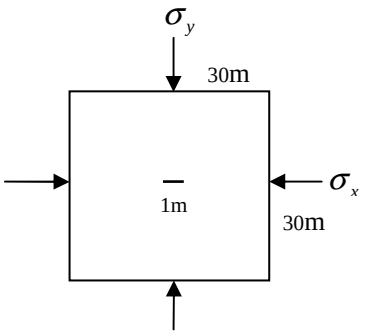

Figure 10: Numerical model for hydraulic fracturing simulation

Mode I. *In situ* stress $(\sigma_x = 1MPa, \sigma_y = 0.5MPa)$

Hydraulic fracturing in homogeneous rock

Initial condition; $p = 1MPa, \Delta p = 0.1KPa, \Delta t = 1s$

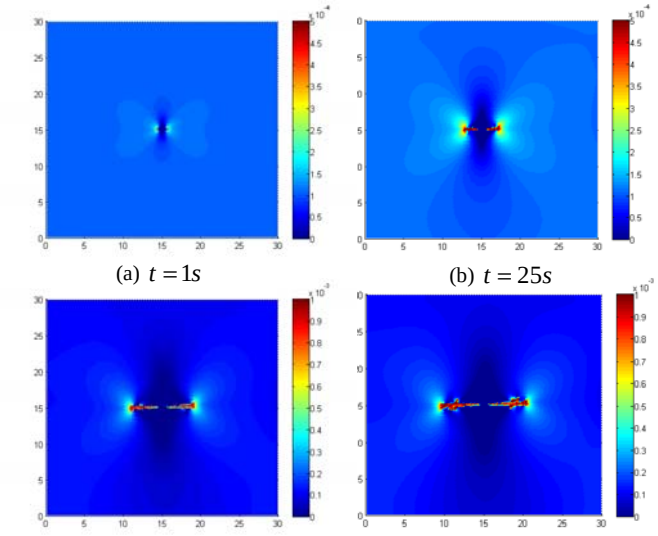

(a) $t = 1s$ (b) $t = 25s$

(c) $t = 35s$ (d) $t = 40s$

Figure 11: Hydraulic fracturing in homogeneous rock (in situ stress $\sigma_x = 1MPa, \sigma_y = 0.5MPa$)

(a), (b) (c), (d) Distribution of principal strain changed along with time

In case of Mode I, *in situ* stress of $\sigma_x = 1MPa, \sigma_y = 0.5MPa$ is applied and initial pressure of $p = 1MPa$, increment of pressure of $\Delta p = 0.1KPa$ and step size of $\Delta t = 1s$ are used. In case of the homogeneous rock, crack propagated toward x-direction because (maximum *in situ* stress direction). In Fig. 12, crack propagates in multiple directions due to stress concentration on weak

elements near the crack tip. These stress concentrations cause multiple fracturing phenomena in heterogeneous reservoir. Effective stress and pore pressure are shown in Fig. 13. Permeability of the crack channel is assumed to be $k = 1md$; as expected, the pore pressure distribution affects the effective stress distribution.

Hydraulic fracturing in heterogeneous rock

Initial condition; $p = 1MPa, \Delta p = 0.1KPa, \Delta t = 1s$

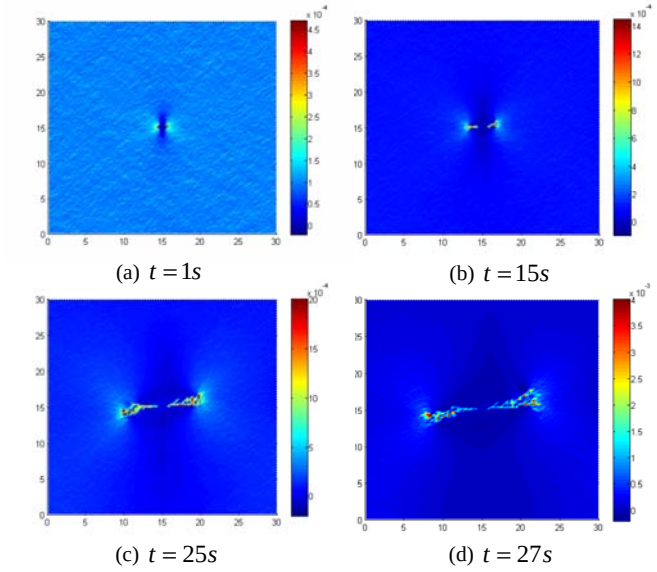

(a) $t = 1s$ (b) $t = 15s$

(c) $t = 25s$ (d) $t = 27s$

Figure 12: Hydraulic fracturing in heterogeneous rock (in situ stress $\sigma_x = 1MPa, \sigma_y = 0.5MPa$)

(a), (b) (c), (d) Distribution of principal strain changed along with time

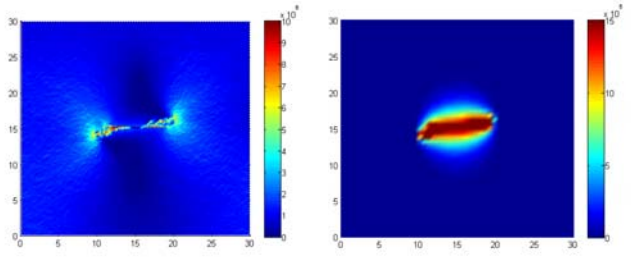

(a) $t = 25s$ (b) $t = 25s$

Figure 13: Hydraulic fracturing in heterogeneous rock (in situ stress $\sigma_x = 1MPa, \sigma_y = 0.5MPa$)

(a) Effective stress distribution at time 25s
(b) Porepressure distribution at time 25s

Mode II. *In situ* stress $\left(\sigma_x = 1MPa, \sigma_y = 3MPa\right)$

Hydraulic fracturing in homogeneous rock

Initial condition; $p = 1MPa, \Delta p = 0.1KPa, \Delta t = 1s$

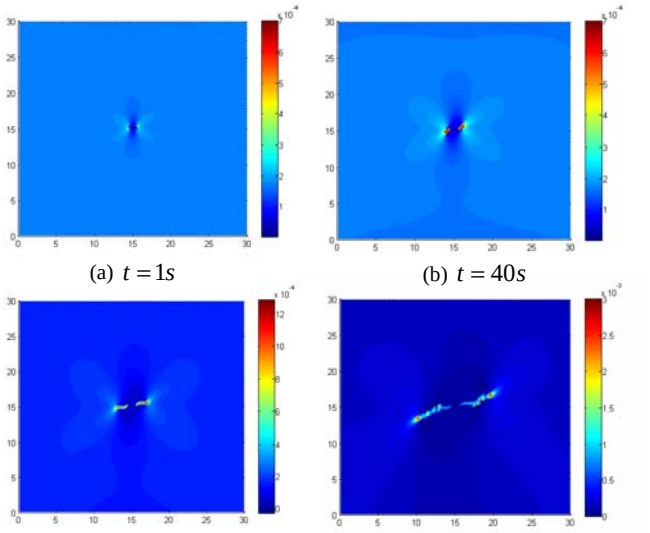

(a) $t = 1s$ (b) $t = 40s$

(c) $t = 50s$ (d) $t = 60s$

Figure 14: Hydraulic fracturing in homogeneous rock (in situ stress $\sigma_x = 1MPa, \sigma_y = 3MPa$)

(a), (b) (c), (d) Distribution of principal strain changed along with time

Hydraulic fracturing in heterogeneous rock

Initial condition; $p = 1.5MPa, \Delta p = 0.1KPa, \Delta t = 1s$

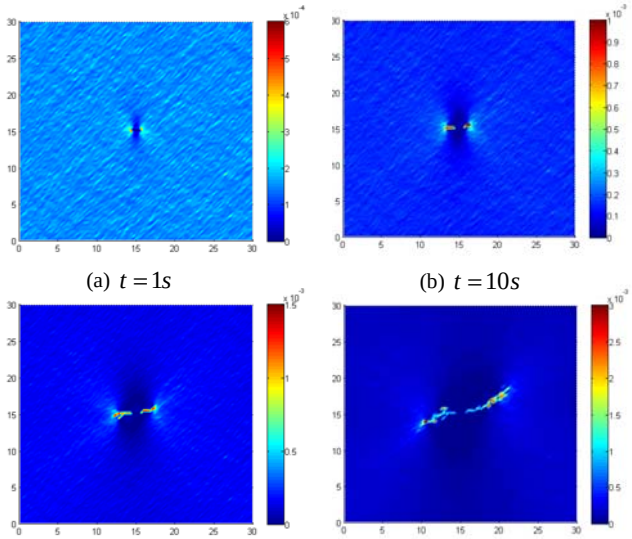

(a) $t = 1s$ (b) $t = 10s$

(c) $t = 15s$ (d) $t = 20s$

Figure 15: Hydraulic fracturing in heterogeneous rock (in situ stress $\sigma_x = 1MPa, \sigma_y = 3MPa$)

(a), (b) (c), (d) Distribution of principal strain changes along with time

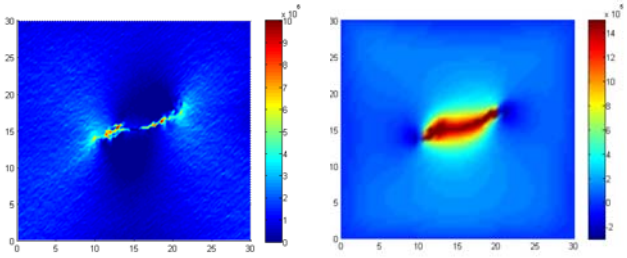

(a) $t = 20s$ (b) $t = 20s$

Figure 16: Hydraulic fracturing in Multi cracks (in situ stress $\sigma_x = 1MPa, \sigma_y = 3MPa$)
(a) Effective stress distribution at time 20s
(b) Porepressure distribution at time 20s

In case of Mode II, *in situ* stress of $\sigma_x = 1MPa, \sigma_y = 3MPa$ and initial pressure of $p = 1MPa$ is applied at increments of $\Delta p = 0.1KPa$; step size of $\Delta t = 1s$ are used. In Fig. 14 and 15, the results show that the crack propagated in the y-direction, i.e., role of *in situ* stress dominates in both homogeneous and heterogeneous reservoir. Fracture tortuosity caused by multiple crack branching phenomena is also observed (Fig. 15). The corresponding effective stress and pore pressure distributions are shown in Fig. 16.

Interaction of Multiple Hydraulic fracturing

Multiple Hydraulic fracturing in heterogeneous rock; I.C. $p = 1MPa, \Delta p = 0.1KPa, \Delta t = 1s$

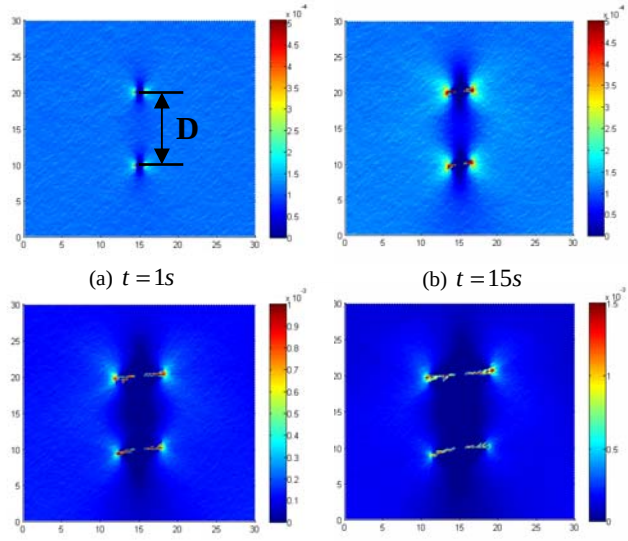

(a) $t = 1s$ (b) $t = 15s$

(c) $t = 25s$ (d) $t = 30s$

Figure 17: Hydraulic fracturing in heterogeneous rock (in situ stress $\sigma_x = 1MPa, \sigma_y = 0.5MPa$)
(a), (b) (c), (d) Distribution of principal strain changes along with time

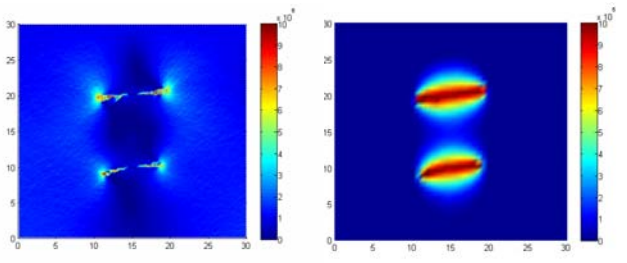

(a) $t = 30s$ (b) $t = 30s$

Figure 18: Hydraulic fracturing in Multi cracks (in situ stress $\sigma_x = 1MPa, \sigma_y = 0.5MPa$)
(a) Effective stress distribution at time 30s
(b) Porepressure distribution at time 30s

In order to study interaction of multiple hydraulic fracturing, a similar test specimen was used except with two initial cracks of length $L = 1m$ (Fig 17). The distance between the two cracks is $D = 10m$. Each hydraulic fracture propagates without interaction until time 25s because the distance $(D = 10m)$ between them prevents their interference. These two fractures start interacting at time 30s, as the pore pressure and displacement fields of each crack affect each other. The interference between the two fractures is shown in Fig. 18. Thus, the interference becomes smaller if the distance between fractures is sufficiently large.

Multiple Hydraulic fracturing in heterogeneous rock; I.C. $p = 1MPa, \Delta p = 0.1KPa, \Delta t = 1s$

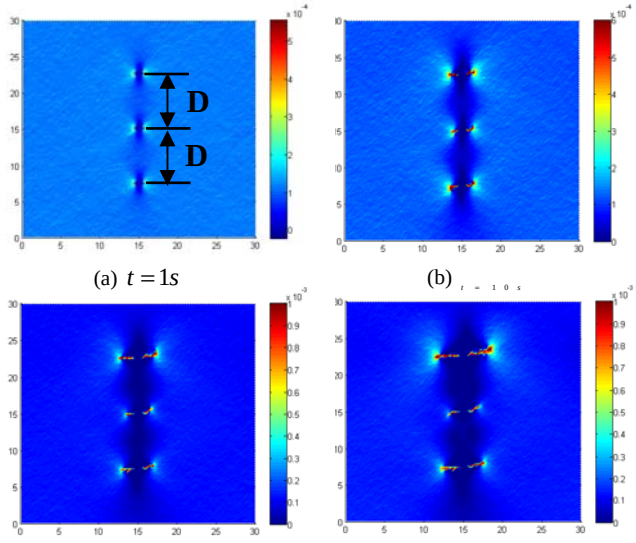

(a) $t = 1s$ (b)

(c) $t = 20s$ (d) $t = 25s$

Figure 19: Hydraulic fracturing in heterogeneous rock (in situ stress $\sigma_x = 1MPa, \sigma_y = 0.5MPa$)
(a), (b) (c), (d) Distribution of principal strain changes along with time

In Fig. 19 and 20 show the interference of multiple hydraulic fractures at a distance of $D = 7.5m$. The propagation of the center fracture was interfered by both upper and lower fractures because of its smaller distance from the other two hydraulic fracturing. The upper fracture is less affected by other fractures, and thus it has a larger crack length. Therefore, the distance between fractures should be determined properly in order to obtain optimal stimulation result.

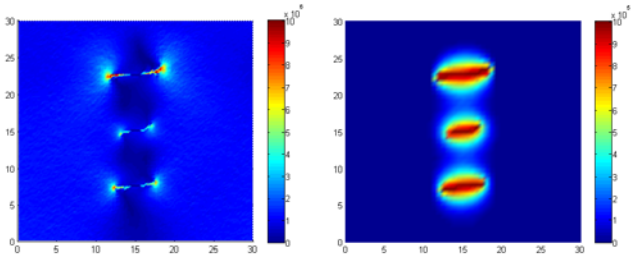

(a) $t = 25s$ (b) $t = 25s$

Figure 20: Hydraulic fracturing in heterogeneous rock (in situ stress $\sigma_x = 1MPa, \sigma_y = 3MPa$)
(a) Effective stress distribution at time 25s
(b) Porepressure distribution at time 25s

Several cases of hydraulic fracturing simulation were studied using the poroelastic VMIB model. In homogeneous rock, hydraulic fractures propagated toward the maximum principal stress direction as the stress tends to be focused on the crack tip. On the other hand, hydraulic fractures in heterogeneous rock propagated in multiple directions because stress concentration occurs on multiple weak elements. Multiple crack branching can clearly be seen in the case of heterogeneous rock in Fig. 12 and 15, while the case of hydraulic fracturing in homogeneous rock did not show multiple cracks (Fig. 11 and 14). Multiple crack branching causes high fracture tortuosity in heterogeneous rock.

CONCLUSION

In this paper, the VMIB model was successfully applied to simulate crack initiation and propagation. Poroelasticity and heterogeneity were applied to the VMIB model using coupled equilibrium equations and the Weibull distribution function. The poroelastic VMIB model for both homogeneous and heterogeneous rock was verified using the Biot's consolidation problem. Also, several hydraulic fracturing problems were simulated with the poroelastic VMIB model. Based on the results of simulations, heterogeneity could cause multiple crack branching and affect the direction of the crack propagation. It is clearly seen that the rock formation becomes weak if mean value of random variable less than 1, so crack opens under lower hydraulic pressure than the homogeneous case. Interference of multiple hydraulic fracturing was studied. Results show that optimal distance between the multiple fractures is required for better production results.

ACKNOWLEDGEMENTS

This project was supported by the U.S. Department of Energy Office of Energy Efficiency and Renewable Energy under Cooperative Agreement DE-PS36-08GO1896. This support does not constitute an endorsement by the U.S. Department of Energy of the views expressed in this publication.

REFERENCES

Biot, M. A. (1941). "General Theory of Three-Dimensional Consolidation." *Journal of Applied Physics*, 12.

Fang, Z., and Harrison, J. P. (2002). "Development of a local degradation approach to the modeling of brittle fracture in heterogeneous rocks." *International Journal of Rock Mechanics & Mining Sciences*, 39, 443-457.

Ganesh Thiagarajan, K. J. Hsia, and Y. Huang. (2003). "Finite element implementation of virtual internal bond model for simulating crack behavior." *Engineering Fracture Mechanics*, 71, 401-423.

Gao, H., and Klein, P. (1997). "Numerical Simulation of crack growth in an isotropic solid with randomized internal cohesive bonds." *Journal of Mechanics, Physics, Solids*, 46, 187-218.

Klein, P., and Gao, H. (1998). "Crack nucleation and growth as strain localization in a virtual-bond continuum." *Engineering Fracture Mechanics*, 61, 21-48.

Potyondy DO., and Cundall PA. (2004). "A bonded-particle model for rock." *International Journal of Rock Mechanics & Mining Sciences*, 41, 1329-64.

T. Wong, Robina. H. C. Wong, K. T. Chau, and C.A. Tang. (2006). "Microcrack statistics, Weibull distribution and micromechanical modeling of compressive failure in rock." *Mechanics of Materials*, 38, 664-681.

Tang, C. A., Tham LG., Lee PKK., Yang TH., and Li LC. (2002). "Coupled Analysis of flow, stress and damage (FSD) in rock failure." *International Journal of Rock Mechanics & Mining Sciences*, 39, 1231-47.

Weibull, W. (1939). "A statistical theory of the strength of materials." *Ing Vetenskaps Akad Handl*, 151, 5-44.

Weibull, W. (1951). "A statistical distribution function of wide applicability." *Journal of Applied Mechanics*, 18, 293-7.

Yuan, S. C., and Harrison, J. P. (2006). "A review of the state of the art in modeling progressive mechanical breakdown and associated fluid flow in intact heterogeneous rock." *International Journal of Rock Mechanics & Mining Sciences*, 43, 1001-1022.

Zhang, Z. N., and Chen, Y. (2008). "Simulation of fracture propagation subjected to compressive and shear stress field using virtual multidimensional internal bonds." *International Journal of Rock Mechanics & Mining Sciences*.

Zhang, Z. N., and Ge, X. R. (2005). "Micromechanical consideration of tensile crack behavior based on virtual internal bond in contrast to cohesive stress." *Theoretical and Applied Fracture Mechanics*, 42, 342-359.

Zhang, Z. N., and Ge, X. R. (2006). "Micromechanical modeling of elastic continuum with virtual multi-dimensional internal bonds." *International Journal for Numerical Method in Engineering*, 65, 135-146.

Zhang, Z. N., and Ghassemi, A. (2010). "The Virtual Multidimensional Internal Bond Method for Simulating Fracture Propagation and Interaction in Poroelastic Rock." *International Journal of Rock Mechanics & Mining Sciences*, In progress.